

# Weather Radar Network Benefit Model for Tornadoes

JOHN Y. N. CHO AND JAMES M. KURDZO

*Lincoln Laboratory, Massachusetts Institute of Technology, Lexington, Massachusetts*

(Manuscript received 7 August 2018, in final form 21 February 2019)

## ABSTRACT

A monetized tornado benefit model is developed for arbitrary weather radar network configurations. Geospatial regression analyses indicate that improvement of two key radar parameters—fraction of vertical space observed and cross-range horizontal resolution—leads to better tornado warning performance as characterized by tornado detection probability and false-alarm ratio. Previous experimental results showing faster volume scan rates yielding greater warning performance are also incorporated into the model. Enhanced tornado warning performance, in turn, reduces casualty rates. In addition, lower false-alarm ratios save costs by cutting down on work and personal time lost while taking shelter. The model is run on the existing contiguous U.S. weather radar network as well as hypothetical future configurations. Results show that the current radars provide a tornado-based benefit of  $\sim \$490$  million (M)  $\text{yr}^{-1}$ . The remaining benefit pool is about  $\$260\text{M yr}^{-1}$ , split roughly evenly between coverage- and rapid-scanning-related gaps.

## 1. Introduction

Excessive heat, tornadoes, and floods are the top three weather causes of fatalities in the United States. In the last 10 years (2008–17) tornadoes have been the number-1 killer (NOAA 2018). Tornado warnings issued by the National Weather Service (NWS) are part of a strategy to reduce casualties by providing people with a chance to shelter in advance (Simmons and Sutter 2011). Forecasters issuing these warnings utilize multiple data sources, with Doppler weather radar serving as the most essential component (Brotzge and Donner 2013). Indeed, the nationwide deployment of the Weather Surveillance Radar-1988 Doppler (WSR-88D) improved tornado warning statistics (Bieringer and Ray 1996) that led to an estimated casualty rate reduction of  $\sim 40\%$  (Simmons and Sutter 2005).

Decreasing tornado casualties is just one of many weather radar benefits to society. These radars, however, are expensive to operate and maintain, and even more so to replace. As the WSR-88Ds approach the end of their original (and upgraded) life spans (NRC 2002), careful consideration must be given to defining requirements for their replacements or further refurbishments to optimize return on investment. Spatial coverage, measurement resolution, update rates, and sensitivity are all important

performance metrics that should be maximized, but there is a cost associated with each. Benefit quantification based on radar performance and network layout can help with difficult decisions and enable objective trade-offs.

This paper presents a geospatial model for monetizing tornado-related benefits of a generic weather radar network. A similar analysis will soon be performed for flash flood warnings for which weather radars also play a key role. These studies support the National Oceanic and Atmospheric Administration (NOAA) as it plans the future of weather radar beyond the WSR-88D. In contemplating advanced technologies such as active phased array radars (e.g., Weber et al. 2007) and/or a denser network of smaller radars (McLaughlin et al. 2009), potential benefits versus costs must be weighed carefully.

The goal of this study was to take as input an arbitrary network of weather radars over a given area, and output a monetized benefit that the radars provide to the area populace with respect to tornadoes. Given that this is a complex problem involving many factors, we endeavored to simplify the model components to only the essentials needed to objectively quantify the radar effects. Statistically insignificant variables were not used. In cases of uncertainty, we took a conservative approach. Because the overwhelming majority of tornadoes in the nation are within the contiguous United States (CONUS), that was

---

*Corresponding author:* John Y. N. Cho, [jync@ll.mit.edu](mailto:jync@ll.mit.edu)

DOI: 10.1175/JAMC-D-18-0205.1

© 2019 American Meteorological Society. For information regarding reuse of this content and general copyright information, consult the [AMS Copyright Policy](#) ([www.ametsoc.org/PUBSReuseLicenses](http://www.ametsoc.org/PUBSReuseLicenses)).

our geographic scope. The model can easily be expanded to include the rest of the United States, but the increase in benefit should be marginal, since we calculated that historically only 0.09% of U.S. tornadoes occur outside the CONUS.

Tornadoes are relatively rare occurrences, and casualties (especially fatalities) are sparser. To achieve statistically significant results, we had to use as many data as we could, which meant including as many years of historical data as possible. However, this imperative was counteracted by the need to maintain a uniform condition set for fair regression results. This issue will be addressed in the individual analysis subsections.

## 2. Radar coverage and performance metrics

In the CONUS, there are 143 operational WSR-88Ds. There are also 44 Federal Aviation Administration (FAA) Terminal Doppler Weather Radars (TDWRs; [Michelson et al. 1990](#)) in the CONUS. The TDWRs' primary mission is providing hazardous wind shear alerts for aircraft landing and taking off at airports. However, their data are also available to forecasters and the public. Relative to the WSR-88D, they provide faster low-level updates (every minute during hazardous weather conditions) and better vertical resolution. However, the TDWR's operation is more negatively impacted by rain attenuation and range-velocity ambiguity issues ([Cho and Weber 2010](#)) because of the utilization of C band rather than S band like the WSR-88D.

In areas with TDWR coverage, do meteorologists make use of this additional radar data for making tornado warning decisions? To answer this question, we conducted a small survey that targeted NWS offices with TDWR coverage, including both tornado-intensive and tornado-sparse locations. We received responses from eight forecast offices (Tampa Bay, Florida; Peachtree City, Georgia; Wilmington, Ohio; Norman, Oklahoma; Fort Worth, Texas; Philadelphia, Pennsylvania; Topeka, Kansas; and Milwaukee, Wisconsin) plus the Storm Prediction Center (SPC). The responses unanimously supported the TDWR as a useful data source for tornado warning decisions. Although the reliance ratio on data from WSR-88Ds and TDWRs varied depending on their relative coverages, one office (Wilmington) asserted that they issued more tornado warnings based on TDWR data than on WSR-88D data. Consequently, we decided to include TDWRs as part of our analysis.

Past studies of tornado warning performance dependence on weather radar have used distance from radar as the key parameter ([Brotzge and Erickson 2009](#); [Brotzge et al. 2011](#); [Brotzge et al. 2013](#)). This makes sense because sensitivity, spatial resolution, and low-level coverage

degrade with range. Tornadoes exist within a limited height above the surface and their rotational signature requires fine horizontal resolution to detect. Our initial investigation into the relationship between radar coverage and tornado warning performance, however, exposed some unexpected behavior at close range. We hypothesized that this was due to not taking into account near-radar degraded coverage caused by the "cone of silence" (e.g., [Fabry 2015](#)). Weather radars do not scan all the way to zenith angle, which leaves an overhead cone of unobserved space. Some of this gap can be covered if there is another radar close enough, but the spatial resolution is degraded. Even if a radar did scan to zenith, it would not be able to measure horizontal velocity as the angle would be too steep.

Why is radar coverage aloft important for tornado warning decisions even though tornadoes occur at the surface? The ultimate goal is to issue a warning before a tornado touches down with as much lead time as possible, and forecasters look for features at both low- and midlevels. For supercell storms, these include a strong mesocyclone, a bounded weak echo region or a hook echo in conjunction with big peak midlevel reflectivities, and a midlevel overhang ([Lemon and Doswell 1979](#); [Falk 1997](#)). Virtually all strong or violent tornadoes are associated with mesocyclones ([Burgess and Lemon 1990](#)). Detection of tornado debris signatures aloft after touchdown is also used for detection and confirmation, with violent tornadoes sending debris to over 18 000 ft (~5.5 km) above ground level (AGL) ([Schultz et al. 2012](#); [Gibbs 2016](#)). The cone of silence cuts off these critical measurements.

Thus, we developed a new radar coverage metric, fraction of vertical volume observed (FVO), with the floor at Earth's surface and ceiling at 20 kft AGL (1 kft = 304.8 m). The top panel of [Fig. 1](#) shows the vertical observation limits versus range for a WSR-88D on a smooth Earth. The bottom plot shows FVO with range, illustrating that this metric combines the cone of silence and Earth curvature effects. In the actual calculation, we included surface elevation data to account for blockage and height AGL variations. We used level-1 Shuttle Radar Tomography Mission (SRTM) data, which includes both natural terrain and surface structures/features, as the primary source of digital elevation, supplemented by level-1 Digital Terrain Elevation Data where SRTM had gaps ([Cho 2015](#)). Our model computation grid matched the horizontal resolution (30 arc s in latitude and longitude) of these datasets, while the vertical grid spacing was 200 ft (~60 m). We employed a 4/3-Earth-radius model for radar frequency propagation path calculations. The minimum elevation coverage angle was taken to be 0° (roughly corresponding to the bottom side

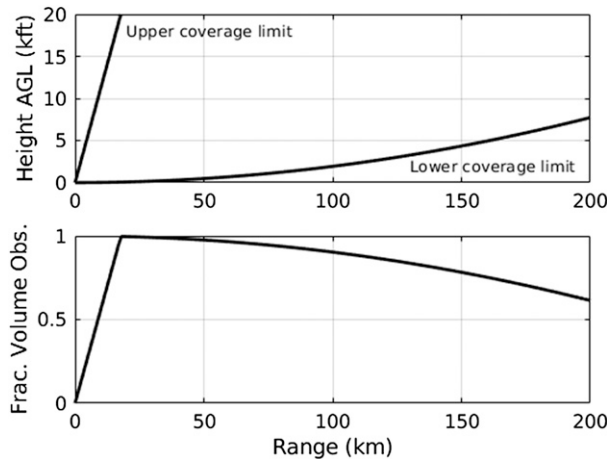


FIG. 1. (Top) WSR-88D vertical coverage limits vs range from radar as delineated by the bottom of the lowest-elevation scan (0) and the top of the highest-elevation scan (20 kft). The 4/3-Earth-radius propagation model is used. (Bottom) Corresponding fraction of vertical volume observed between 0 and 20 kft AGL.

of the main lobe) for both WSR-88D and TDWR while the maximum angle was set to  $20^\circ$  for WSR-88D and  $60^\circ$  for TDWR (topside of the main lobe). These are approximations, since the minimum and maximum angles vary from site to site (especially for TDWRs) and for different scan strategies (especially for WSR-88Ds).

Figure 2 shows the resulting FVO over the CONUS for the combined WSR-88D and TDWR networks. The 20-kft value for the FVO ceiling was chosen as a compromise between weighting the near-surface observations too much and placing equal weighting on all observable altitudes. Although 20 kft is somewhat arbitrary, the fact that FVO is a fractional metric

ameliorates hard cutoff effects. We also tried varying the ceiling height to probe the model sensitivity to this value. The annual tornado casualty estimate for today's weather radar network (discussed in section 4) turned out to be lower by 0.3% with a 10-kft FVO ceiling and lower by 0.01% with a 30-kft FVO ceiling when compared with the 20-kft-FVO-ceiling case. Thus, the model sensitivity to this parameter appeared to be very small above 20 kft. In any case, all three casualty estimates were within the error bars of the actual average annual tornado casualties.

We also considered the cross-radial horizontal resolution (CHR). This parameter is important for detection of tornadic velocity couplets (Wood and Brown 1997; Brown et al. 2002; Brown and Wood 2012b). Along-range horizontal resolution is also a factor but is not an interesting metric, because it is a constant value everywhere for monostatic radars. In rough terms, CHR is angular resolution (in radians) multiplied by range. Angular resolution is dependent on the antenna beamwidth and the dwell size (Zrníc and Doviak 1976). Although the TDWR's beamwidth is about one-half that of the WSR-88D's ( $0.55^\circ$  vs  $1^\circ$ ), because its sampling interval is  $1^\circ$ , the effective angular resolution of the two systems are not very different. Currently, the WSR-88D has a so-called superresolution mode that outputs data at overlapping  $0.5^\circ$  intervals, but the effective angular resolution is still  $\sim 1^\circ$  based on the data window and the beamwidth (Torres and Curtis 2006). Therefore, we approximated the angular resolution of both systems as  $1^\circ$ . The resulting CHR is, thus, functionally the same as the distance-from-radar metric for the current radars. Future radars, however, could have very different angular resolutions, for example, a dense network of broad-beam

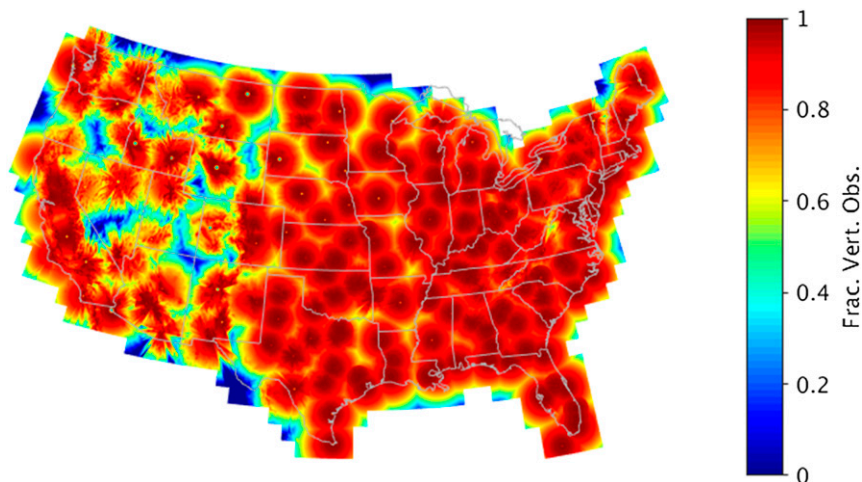


FIG. 2. Fraction of vertical volume observed between 0 and 20 kft AGL by current CONUS WSR-88Ds and TDWRs.

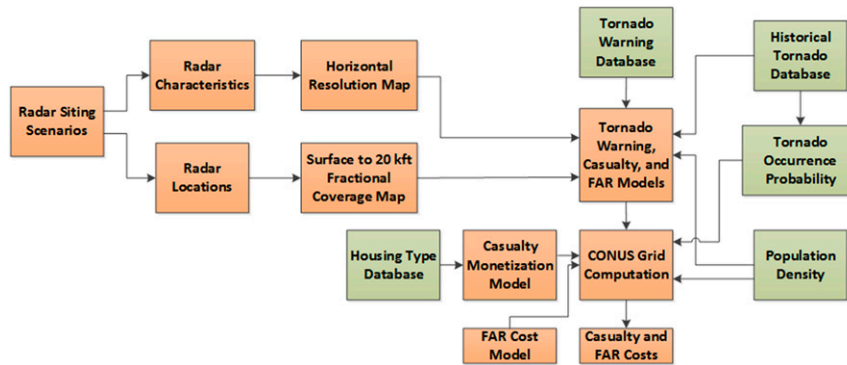


FIG. 3. Block diagram of weather radar network benefit model for tornado warnings.

systems (Brotzge et al. 2010), or even angle-dependent resolution for fixed planar phased arrays (Brown and Wood 2012a), which may make CHR a more meaningful performance yardstick.

### 3. Model development

Tornado warnings are expected to benefit society by allowing people to shelter in advance of impact, thereby reducing casualties. This intuitive causal chain has been proven empirically, at least for the case of injuries (Simmons and Sutter 2008); fatalities are such rare events that it is difficult to achieve statistically significant results for them. Little can be done to protect property at warning time scales, so we only considered casualty reduction in our model. At the same time, there is a cost incurred for those taking shelter based on the loss of work and personal time. If false alarms can be decreased, some of this cost could be recouped (section 3g).

Better Doppler weather radar coverage should contribute to tornado casualty reduction by improving tornado warning performance. It may also lower sheltering cost by decreasing false alarms. Our benefit model combined all of these effects to output a monetized cost given an arbitrary weather radar network as input (Fig. 3).

#### a. Detection probability dependence on radar coverage

A 5-yr (2000–04) study (Brotzge and Erickson 2010) showed that the fraction of tornadoes without warning increased with distance from radar, which implies that better radar coverage improves tornado warning performance. We performed our own analysis using NWS tornado warning data, extending the analysis period. National deployment of operational WSR-88Ds was completed in late 1997. Therefore, we set the analysis period to be between 1 January 1998 and 31 December 2017.

However, after 1998, two new WSR-88D sites were added—Evansville, Indiana (operational January 2003), and Langley Hill, Washington (installed September 2011). Furthermore, the TDWR Supplemental Product Generator (SPG) deployment (Istok et al. 2009), which enabled TDWR data access by NWS forecasters, was finished in late 2008. Thus, to account for these radar network changes, we generated four sets of FVO and CHR maps: 1) prior to the Evansville WSR-88D installation, 2) after the Evansville addition but before the TDWR SPG deployment, 3) after TDWR SPG but before the Langley Hill WSR-88D installation, and 4) after the Langley Hill deployment. We did not discriminate between the periods before and after the WSR-88D dual-polarization upgrade, since overall tornado warning statistics did not improve postupgrade in our analysis. This method is not perfectly accurate, because we did not take into account the exact periods of radar down times, variations in volume-scanning strategies, etc., but the expansion of the analyzed database to 20 years helped to suppress the noise level of these minor errors relative to the desired signal.

Tornado event data were downloaded from the storm events database (<https://www.ncdc.noaa.gov/stormevents/>) of NOAA's National Center for Environmental Information. Tornado warning data were obtained from the Iowa Environmental Mesonet NWS Watch/Warnings archive (<https://mesonet.agron.iastate.edu/request/gis/watchwarn.phtml>). A warning was deemed to be a hit if any portion of the tornado path was inside the area enclosed by the warning latitude–longitude coordinates and if any part of the tornado existence period overlapped the warning valid interval; otherwise, the warning was classified as a false alarm. For a hit, the lead time was calculated as the tornado start time minus the initial time of warning issuance. Multiple warnings for one storm were treated separately. For the remainder of the paper, we will refer to the fraction of tornadoes with warning as the probability of detection (POD), which is

TABLE 1. CONUS tornado warning statistics for the analysis period for the six EF categories.

	0	1	2	3	4	5
Tornado count	15 872	8376	2543	780	171	19
Fraction with warning	0.67	0.70	0.84	0.95	0.98	1.0

the more commonly used term. The number of tornadoes and POD during the analysis period, parsed by enhanced Fujita scale (EF) number, are given in Table 1.

Note that prior to 1 February 2007, the original Fujita scale was used to rate tornadoes. With a far greater number of damage indicators used, the EF is agreed to be a more accurate and consistent estimator of tornado strength. Although carefully designed to minimize discontinuity in the historical tornado database, there may still be some small statistical differences between the old and new scales, such as shifts in the relative distributions between strength categories (Edwards and Brooks 2010), which could potentially affect our regression results.

For each tornado event, FVO and CHR at the start-of-tornado location were recorded. Based on similarities in POD statistics, and also to increase the number of samples per category for the high-EF cases, we then computed POD versus FVO and CHR for EF0–1, EF2, and EF3–5. For these calculations, FVO was binned into the following intervals: [0, 0.3], (0.3, 0.6], (0.6, 0.7], (0.7, 0.8], (0.8, 0.9], and (0.9, 1], while CHR (in meters) was binned into: [0 500], (500, 1000], (1000, 1500], (1500, 2000], (2000, 2500], and (2500, ∞).

Figures 4–6 show POD versus FVO for EF0–1, EF2, and EF3–5. The plotted abscissa values are the means of the binned FVO data, not the center of the bins. The horizontal error bars are ±1.96 times the FVO standard deviation divided by the square root of the number of data points. The vertical error bars are ±1.96 times the standard error for proportional data (the computed PODs) divided by the square root of the number of data points. These bars indicate the 95% confidence intervals in both dimensions. A minimum of four data points per bin were required for inclusion in the plots, which eliminated low-FVO points with increasing EF number.

POD increases with FVO for all EF categories. This is a key result, as it associates improvement in tornado warning performance to better radar coverage. We modeled these dependencies with least squares straight line fits to the data with input uncertainty in two dimensions using the *Numerical Recipes* function “fitxy” (Press et al. 1992). Results of the fitting are listed in Table 2, where  $a$  is the y intercept,  $b$  is the slope,  $\sigma_a$  is the standard deviation of  $a$ ,  $\sigma_b$  is the standard deviation of  $b$ ,  $\chi^2$  is the final chi-square value, and  $Q$  is the goodness-of-fit probability. The slopes are positive; they remain

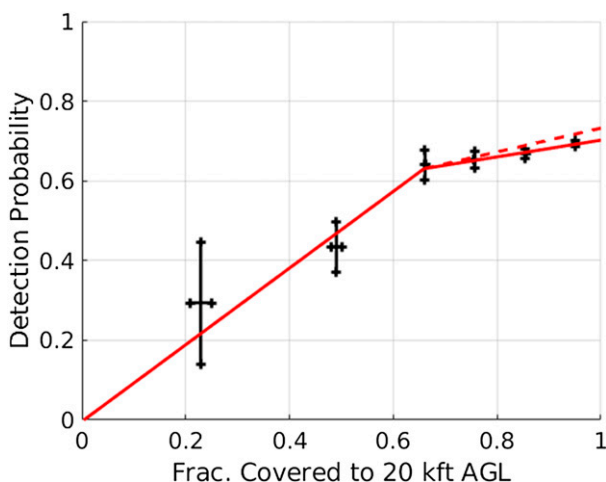


FIG. 4. Fraction of EF0 and EF1 tornadoes warned vs fraction of vertical volume covered by radar from surface to 20 kft AGL. Solid red lines are least squares linear fits to the data. The dashed red line corresponds to the rapid-scanning-radar case.

positive within the errors except for EF3–5, which has essentially zero slope. The dashed red line in Fig. 4 will be explained in section 3e.

We defined a tornado with warning to include those with zero and negative lead times, because even if a tornado touches down before the warning issuance time, as long as the warning is issued before the end of the event, people farther down the track have a chance to shelter before impact. Still, we reran the analysis to include only positive lead times as a sensitivity check. The main effect of excluding zero and negative lead times was to lower the POD values (warning performance) as expected, but POD still clearly increased with FVO for

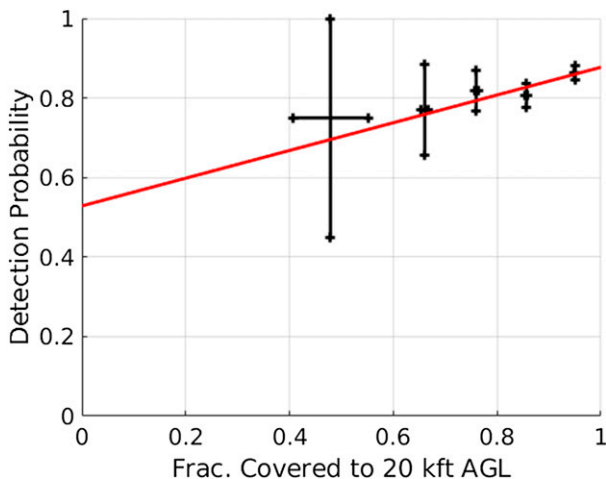


FIG. 5. Detection probability of EF2 tornadoes vs fraction of vertical volume covered by radar from surface to 20 kft AGL. The red line is a least squares linear fit to the data.

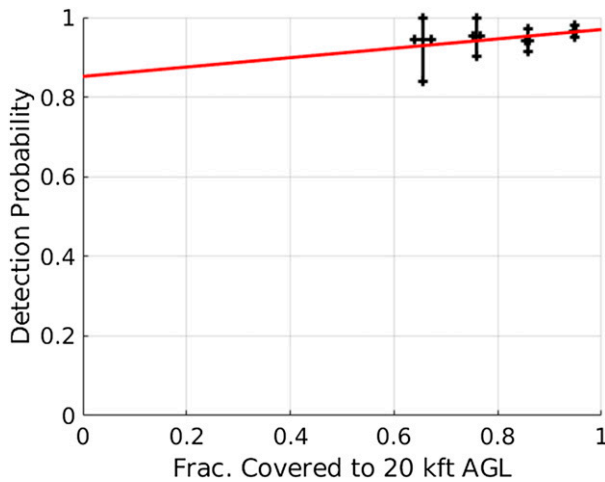


FIG. 6. As in Fig. 5, but for EF3, EF4, and EF5 tornadoes.

all EF groups and the linear fits were significant. The slopes (again, all positive) of the fitted lines agreed with the case including zero and negative lead times within their respective uncertainties.

The dependence of POD on CHR was more problematic, as POD did not decrease monotonically with increase in CHR. Figure 7 shows the results for all EF categories combined. Since CHR is proportional to distance from the nearest radar, the decrease in POD at close range may be at least partly due to the negative impact of the cone of silence. This type of cross contamination of effects is undesirable, since future radar systems could have a significantly smaller cone of silence and a CHR–POD relationship based mostly on WSR-88D data may not hold. Therefore, we excluded CHR as a radar performance metric from the POD dependency model.

#### b. Dependence of false-alarm ratio on radar coverage

Tornado warning false-alarm ratio (FAR) depends on many factors, for example, time of day, population density, and tornado occurrence frequency. An earlier 5-yr study (2000–04) showed FAR to be more or less constant with distance from radar up to  $\sim 150$  km, but then decreasing at farther ranges (Brotzge et al. 2011). Taken at face value, this meant that improving radar coverage would not lower FAR, and might even raise the overall number of false alarms. It is also possible that lower FAR (and lower POD) might result from forecasters' reluctance to issue warnings where they know radar coverage is poor. Thus, we revisited this study using the FVO and CHR radar coverage metrics instead of distance from radar, and expanded the database period as we did for the POD dependency analysis in section 3a.

TABLE 2. POD vs FVO linear fit results, categorized by EF groupings.

	0–1		2	3–5
	Low FVO	High FVO	All FVO	All FVO
$a$	0.00	0.49	0.53	0.85
$b$	0.96	0.21	0.35	0.12
$\sigma_a$	0.18	0.07	0.19	0.18
$\sigma_b$	0.31	0.09	0.25	0.32
$\chi^2$	0.56	0.24	0.82	0.22
$Q$	0.46	0.89	0.84	0.89

An important point about the database is that operational NWS tornado warnings switched from a county-based to a storm-based polygon area definition on 1 October 2007. This transition made a large difference in the warning statistics as seen in Table 3, with the mean warning area shrinking to  $\sim 40\%$  of the former mean area. Because the analysis of FAR versus the radar coverage metrics involved computation of the average coverage parameters over the warning area, the change to storm-based warning resulted in much sharper relationships. This was in contrast to the POD analysis of section 3a, which used the location of the tornado with the radar coverage values, not the warning area. Therefore, in this section, we only used the database period 1 October 2007 to 31 December 2017.

For the FAR versus radar coverage calculations, FVO was binned into the following intervals:  $[0, 0.3]$ ,  $(0.3, 0.5]$ ,  $(0.5, 0.7]$ ,  $(0.7, 0.8]$ ,  $(0.8, 0.9]$ , and  $(0.9, 1]$ , while CHR (in meters) was binned into:  $[0, 600]$ ,  $(600, 1300]$ ,  $(1300, 2100]$ ,  $(2100, 3000]$ ,  $(3000, 4000]$ , and  $(4000, \infty)$ . Limits were adjusted to spread out the data distribution more evenly among bins. The results and subsequent linear fits are plotted in Fig. 8 (FAR vs FVO) and Fig. 9 (FAR

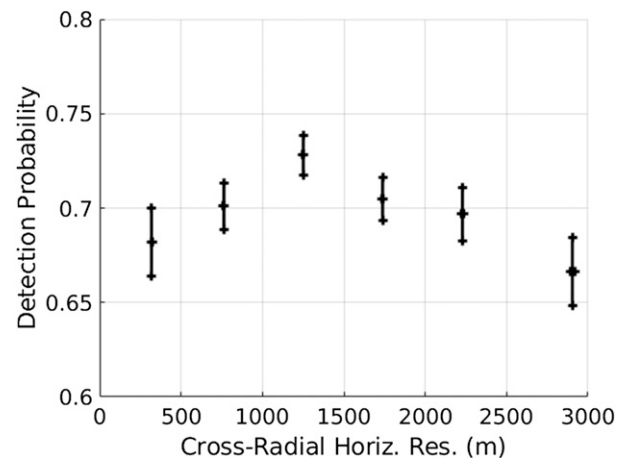


FIG. 7. Tornado detection probability vs cross-radial horizontal resolution of radar observations.

TABLE 3. Tornado warning statistics before and after switch to storm-based warnings.

Period	1 Jan 1998– 30 Sep 2007	1 Oct 2007– 31 Dec 2017
Warning count	33 814	23 717
Mean warning area	2370 km <sup>2</sup>	967 km <sup>2</sup>
FAR	0.763	0.722

versus CHR); the fitting procedure was the same as for Figs. 4–6 as explained in section 3a. For Fig. 9, the line fit excluded the rightmost data point, and the FAR was capped at 0.76 as shown by the horizontal red line, a piecewise linear approximation of what appears to be a saturation curve type of behavior. The dashed red line will be explained in section 3e.

Curiously, in this case, FAR versus CHR yielded the better fit. Coefficients and fitting statistics are given in Table 4. In an attempt to optimally combine CHR and FVO in the FAR-radar coverage model, we tried weighted means of the two linear relationships and compared the resulting errors (mean-squared sums of the difference between model and data). The smallest error was achieved with zero weighting on the FVO relationship. Thus, only the FAR–CHR relation was used in our model.

c. Casualty dependence on tornado warning

Now that we have established models for dependency of tornado warning performance on radar coverage, we move on to discuss casualty dependence on tornado warnings. Tornado casualty rate is positively correlated with surface dissipation energy, population density, fraction of mobile homes in housing stock, and FAR (Simmons and Sutter 2009; Fricker et al. 2017). The dependence on historical FAR is likely due to “the boy who cried wolf” effect, where residents used to a high FAR are less likely to heed warnings seriously and take shelter. Tornado casualty rate is negatively correlated with the presence of tornado warnings, as expected; when a tornado warning is correctly issued, one intuitively that lead time should also be negatively correlated with casualty, but this has not been established, as the dependence of casualty rate on lead time is not monotonic (Simmons and Sutter 2008). Time-based variables like season and time of day were also shown to be significant predictors of casualty rate, but these are not factors that we can use in our time-independent cost generation model, so we did not consider them.

Since casualty is a counting variable and its statistical distribution is overspread, we followed the earlier studies in assuming a negative binomial distribution model,

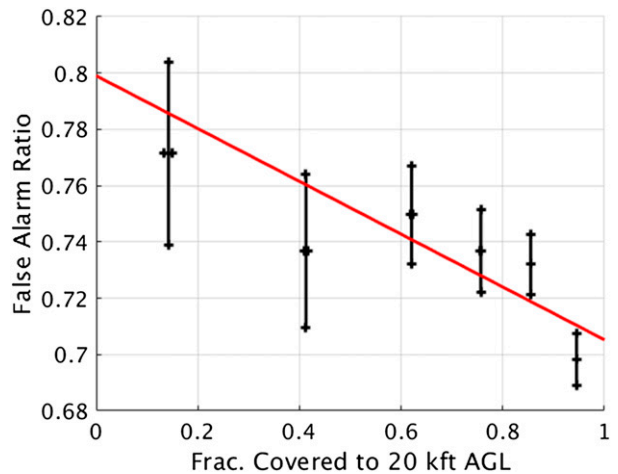


FIG. 8. Tornado warning false-alarm ratio vs fraction of vertical volume covered by radar from surface to 20 kft AGL. The red line is a least squares linear fit to the data.

$$C \sim \text{NegBin}(\mu, \theta), \tag{1}$$

where  $C$  is conditional casualty count,  $\mu$  is the distribution mean, and  $\theta$  is the dispersion parameter (Simmons and Sutter 2008; Fricker et al. 2017). Our regression model is expressed as

$$\ln \mu = \alpha \ln P_T + \beta \ln S + \gamma M + \delta F_0 + \varepsilon W + k, \tag{2}$$

where  $P_T$  is population inside the tornado path,  $S$  is tornado surface dissipation energy density,  $M$  is fraction of  $P_T$  residing in mobile homes, recreational vehicles, and vans,  $F_0$  is mean historical FAR inside the tornado path,  $W$  is warning presence (0 for absent; 1 for present),  $k$  is the intercept constant, and  $\alpha, \beta, \gamma, \delta,$  and  $\varepsilon$  are the

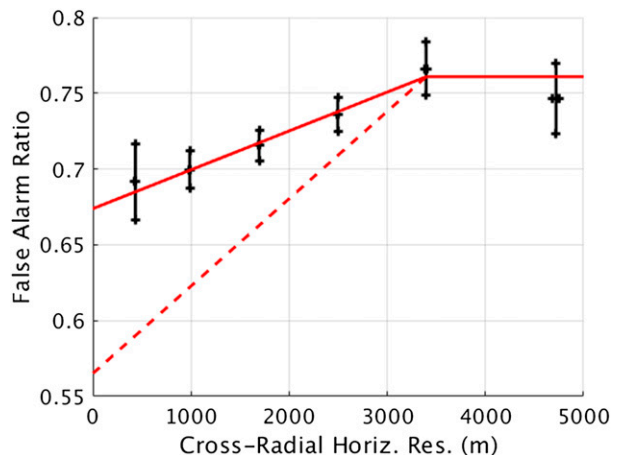


FIG. 9. Tornado warning false-alarm ratio vs mean cross-radial horizontal resolution of radar observations. The sloped solid red line is a least squares linear fit to the first five data points. The dashed red line corresponds to the rapid-scanning-radar case.

TABLE 4. FAR vs radar coverage parameter linear fit results.

Parameter	FVO	CHR
$a$	0.80	0.67
$b$	-0.094	$2.6 \times 10^{-5} \text{ m}^{-1}$
$\sigma_a$	0.026	0.015
$\sigma_b$	0.033	$7.4 \times 10^{-6} \text{ m}^{-1}$
$\chi^2$	4.8	0.22
$Q$	0.30	0.97

regression coefficients. The tornado surface dissipation energy density is (Fricker et al. 2017)

$$S = \rho \sum_{m=0}^5 w_m v_m^3, \quad (3)$$

where  $\rho$  is the air density (assumed to be  $1 \text{ kg m}^{-3}$ ),  $v$  is the midpoint wind speed for each EF value  $m$ , and  $w$  is the corresponding fraction of the path area. Because there is no upper bound speed for EF5, we set a midpoint of  $97 \text{ m s}^{-1}$  following Fricker et al. (2017). Path area fractions are not given in the tornado database, so mean  $w_m$  values were taken from Table 3-1 of Ramsdell and Rishel (2007).

In (2) it is not intuitively obvious that population should be used instead of population density or that dissipation energy density should be used instead of dissipation energy; Fricker et al. (2017) opted for population density and dissipation energy. Both terms should not be posed as density, since that would omit the important tornado path area factor. We chose to use the combination that gave the best regression fit, and that was dissipation energy density and population.

We did not separate casualties into fatalities and injuries at this stage, as the former is merely the extreme end case of the latter. By combining the two groups, we avoided the problem of extremely sparse statistics for fatalities. Only direct casualties were included to tighten the causal relationship between the tornado and its impact on people. In the monetization stage (section 3d), we parsed the model results into fatalities and two types of injuries.

For population data, we obtained gridded population density from the Center for International Earth Science Information Network (CIESIN 2017). The latitude-longitude resolution of these data matched our model grid spacing of 30 arc s. Data were available for 2000, 2005, 2010, 2015, and 2020 (projected). For 1998–99 we used the 2000 data, and for other years we linearly interpolated as needed between the available years.

Mobile-housing statistics were pulled from the American Community Survey database for 2015 (USCB 2016) and the Decennial Census for 2000 (Manson et al. 2018).

TABLE 5. Tornado casualty model regression results for two data periods.

Parameter	Estimate	Std error	$z$	$\text{Pr}( >  z  )$
1 Jan 1998–31 Dec 2017				
$\alpha$	0.296	0.0146	20.2	$< 2 \times 10^{-16}$
$\beta$	6.29	0.159	39.5	$< 2 \times 10^{-16}$
$\gamma$	1.48	0.242	6.10	$1 \times 10^{-9}$
$\delta$	0.579	0.159	3.63	0.0003
$\epsilon$	-0.815	0.0796	-10.2	$< 2 \times 10^{-16}$
$k$	-70.3	1.71	-41.1	$< 2 \times 10^{-16}$
$\theta$	0.122	0.004 91	—	—
1 Oct 2007–31 Dec 2017				
$\alpha$	0.315	0.0219	14.4	$< 2 \times 10^{-16}$
$\beta$	6.14	0.237	26.0	$< 2 \times 10^{-16}$
$\gamma$	1.31	0.348	3.77	0.0002
$\delta$	0.622	0.208	2.99	0.003
$\epsilon$	-0.556	0.118	-4.70	$3 \times 10^{-6}$
$k$	-69.1	2.54	-27.2	$< 2 \times 10^{-16}$
$\theta$	0.115	0.006 94	—	—

The population in housing units were broken down by building structure categories, one of which was “mobile home.” We grouped this together with the much smaller “boat, RV, van, etc.” category to arrive at our mobile-housing population. The highest spatial resolution data available (block group level) were normalized by the total population in each block group to yield the fraction of population in mobile housing. This dataset was then sampled and mapped to our latitude-longitude grid to generate the CONUS maps. In the regression analysis, the 2000 map was used for 1998–2000, the 2015 map was used for 2015–17, and linearly interpolated maps (between 2000 and 2015) were used for 2001–16. Although only 5.8% of the national population lives in mobile housing, because they are prevalent in rural regions, disproportionately large areas of the country have significantly higher fractions.

From the tornado warning data, we computed CONUS maps of historical FAR on our model grid for the periods before and after storm-based warnings. Areas with no data were dropped from the regression analysis.

We used the function “glm.nb” from the open statistical analysis software package R (<https://www.R-project.org/>) for the negative binomial regression analysis. The results are given in Table 5. All coefficients estimates had the expected signs; that is, mean casualty per tornado was positively correlated with population, tornado dissipation energy, and FAR, and was negatively correlated with the presence of tornado warning. The coefficient signs were constant within the standard errors, and the  $z$  statistics showed that all coefficient estimates were significant at a much better than 0.001 level. Furthermore, comparing models with and without each variable through degree-of-freedom chi-square tests



TABLE 6. Mean CONUS tornado statistics vs EF number.

EF	Fatality fraction	Path area (km <sup>2</sup> )	Surface dissipation energy density (GW km <sup>-2</sup> )
0	0.021	0.0274	37.6
1	0.047	0.347	48.2
2	0.053	1.67	64.8
3	0.067	5.86	85.2
4	0.067	11.9	96.8
5	0.15	29.3	114

indicated that every variable was a statistically significant predictor of casualty rate.

Regression analysis was performed on all data as well as data since the implementation of storm-based warnings. Comparison of Table 5 values shows that the results were quite robust relative to this data segmentation. Since the error and significance statistics were better for the full dataset, we adopted those results in our benefit model. Application of (2) with the estimated coefficients to the same input data yielded a casualty count of 14 970 as compared with the actual count of 15 611, which is a difference of less than 5%. According to this model, the presence of a tornado warning reduces casualty by 55%.

#### d. Casualty monetization

In benefit studies like this one, the value of a statistical life (VSL) is often used to monetize casualties. VSL is an estimate of one's willingness to pay for small reductions in mortality risks. We adopted the U.S. Department of Transportation's (DOT) guidance (Moran and Monje 2016), which called for a VSL of \$9.6 million (M) in 2015 dollars. To adjust the value to 2018 dollars, we employed the DOT's formula,

$$\text{VSL}_T = \text{VSL}_0 \frac{\text{CPI}_T}{\text{CPI}_0} \left( \frac{\text{MUWE}_T}{\text{MUWE}_0} \right)^q, \quad (4)$$

where CPI is the consumer price index, MUWE is the median usual weekly earnings,  $q$  is income elasticity, and the subscripts  $T$  and  $0$  denote updated base year and original base year, respectively. From the U.S. Bureau of Labor Statistics (BLS) online database, we obtained  $\text{CPI}_T/\text{CPI}_0 = 1.0606$  ([https://www.bls.gov/data/inflation\\_calculator.htm](https://www.bls.gov/data/inflation_calculator.htm)) and  $\text{MUWE}_T/\text{MUWE}_0 = 1.0571$  (<https://www.bls.gov/cps/cpswktabs.htm>) for a baseline of January 2015 and updated time of January 2018. With the DOT's estimate of  $q = 1$ , we got a 2018 VSL of \$10.8M.

As discussed in section 3c, our casualty regression model did not differentiate between fatalities and injuries. To parse the model output into the two types of casualty, we relied on the strong relationship between

TABLE 7. Casualty cost by type. Here and below, \$M indicates millions of U.S. dollars.

Casualty type	Cost (\$M)
Fatality	10.8
Injury (hospitalized)	2.86
Injury (treated and released)	0.506

EF category and relative proportions of casualty types computed from the tornado database. Table 6 gives the mean fraction of casualties that are fatalities versus EF number.

Injuries can be monetized as fractions of VSL. To do this, we referenced a Federal Emergency Management Administration (FEMA) tornado safe room benefit study (FEMA 2009). Their formulation specified injuries requiring hospitalization as level 4 (severe) and injuries that led to professional treatment and immediate release as level 2 (moderate). The latest DOT guidance sets the level-4 injury cost at  $0.266 \times \text{VSL}$  and level-2 injury cost at  $0.047 \times \text{VSL}$  (Moran and Monje 2016). In 2018 dollars, these costs are \$2.86M and \$0.506M, respectively. All estimated casualty costs are compiled by type in Table 7.

The historical tornado database does not differentiate injuries by severity. Thus, we needed another way to generate model output for injuries requiring hospitalization versus those that are treated and released. Fortunately, the FEMA report connected the probability of injury levels to tornado EF class and building type. We simplified the building categories to two (mobile housing and other) to match the gridded fraction of population in housing data that we obtained for the regression analysis. For the "other" category, we averaged the FEMA table values for one- and two-family residences and institutional buildings (Table 8). The results were used to generate CONUS maps for the fraction of injuries requiring hospitalization by EF number; an example (for EF3) is presented in Fig. 10.

#### e. Rapid-scan benefits

Faster radar measurement updates could improve tornado warning lead time, POD, and FAR (Heinselman et al. 2015). However, weather radar volume update rate is constrained by the need to collect enough samples over the same space to reduce measurement error and improve clutter filtering, as well as by the limited agility of the antenna. WSR-88D volume coverage patterns (VCPs) designed for convective conditions have periods of 4.5–6 min, whereas TDWR hazard mode volume scans have ~2.5-min periods (albeit with sparse sampling in elevation angle) and a 1-min update time for base scans. In 2011, the automated volume scan evaluation and

TABLE 8. Injury-type fraction vs EF number and building type.

Building type	EF	Treat and release	Hospitalize
Manufactured (mobile homes)	0	0.89	0.11
	1	0.65	0.35
	2	0.35	0.65
	3	0.25	0.75
	4	0.25	0.75
Others	5	0.25	0.75
	0	1.00	0.00
	1	0.67	0.33
	2	0.65	0.35
	3	0.55	0.45
	4	0.43	0.57
	5	0.29	0.71

termination (AVSET) algorithm was deployed on WSR-88Ds to adaptively shorten a VCP by skipping high-elevation cuts with no weather, and in 2014, the supplemental adaptive intravolume low-level scan (SAILS) technique was introduced, giving operators the option to run an additional base scan during the middle of a VCP (Chrisman 2013). Subsequently, a multiple-elevation scan option for supplemental adaptive intravolume low-level scan (MESO-SAILS) was added in 2016 to allow the insertion of multiple base scans within a VCP period (Chrisman 2014).

These new VCP algorithms allow better update rates in the elevation angles targeted for specific weather phenomena such as potentially tornadic storms. The scan rates are still ultimately limited by the radar resource. In the future, significantly faster updates could be enabled by operational deployment of electronically scanned phased array radars (e.g., Weber et al. 2007; Heinselman et al. 2008). Since we wish to apply our

model to potential future radar networks, we need to quantify added benefits from rapid scanning.

Although lengthening tornado warning lead times should help lower casualties, this connection has not been clearly established (Simmons and Sutter 2008). Our analysis also did not yield a statistically meaningful result to support this position. Thus, we did not pursue this path for modeling rapid-scanning benefits. However, we showed that improvements in tornado warning POD and FAR can reduce casualty rates. Furthermore, previous studies have indicated that faster radar scanning can raise POD and lower FAR (Heinselman et al. 2015; Wilson et al. 2017). Therefore, combining the two dependencies, we were able to model the casualty-reduction benefits of rapid-scan radars.

The National Weather Radar Testbed (NWRT) (Heinselman and Torres 2011) was used in a series of phased array radar innovative sensing experiments (PARISE) to study the effects of faster scanning on weather forecasters making severe storm warning decisions. Tornadoes resulting from three storm types (squall line, supercell cluster, and supercell) were studied in the 2015 PARISE (Wilson et al. 2017), with surveillance volume update periods of 61–76 s. The radar data were sampled to generate full- (~1 min), half- (~2 min), and quarter- (~5 min) speed outputs. Each temporal resolution set was given to a separate group of 10 NWS forecasters for warning guidance. The quarter-speed case is representative of most of the weather radar data used in our regression analyses and thus can be considered to be the baseline condition.

The supercell case yielded no difference among the three groups, with a perfect score of  $POD = 1$  and  $FAR = 0$  across the board. The squall line case also showed little variation with update rate, with  $FAR = 1$

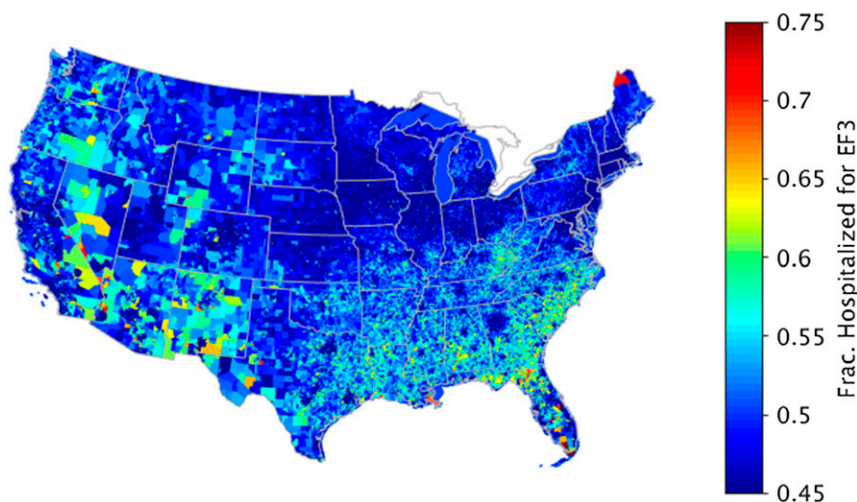


FIG. 10. Modeled fraction of EF3 tornado injuries that require hospitalization.

for all groups,  $POD = 0.1$  for the full- and half-speed groups, and  $POD = 0$  for the quarter-speed group. The supercell cluster case generated the only notable response with  $POD$  increasing—0.1, 0.6, and 0.8—and  $FAR$  decreasing—0.50, 0.53, and 0.33—for the quarter-, half-, and full-speed groups, respectively.

Since these results were based on a very small sample size (30 forecasters working on one null storm case and three storms that spawned five tornado events in total), we applied them conservatively. PARISE was conducted under fairly ideal radar coverage, so looking at Figs. 4–6, we only considered changing the  $POD$  versus  $FVO$  relationship close to  $FVO = 1$ . Since the maximum  $POD$  enhancement of 0.8 (at full scan rate) only exceeded the model values at  $FVO = 1$  for the EF0–1 case, that was the only modeled relationship modified for the rapid-scan case. In other words, the  $POD$  performance of the EF2 and EF3–5 cases were already too good for a rapid-scan capability to add value. For 1-min update scans, we enhanced the  $POD$ -versus- $FVO$  relationship as indicated by the dashed line in Fig. 4. The new value of  $POD$  at  $FVO = 1$  is given by  $0.8u + (a + b)(1 - u)$ , where  $a$  and  $b$  are taken from the EF0–1 high- $FVO$  column in Table 2, and  $u = 0.316$  is the fraction of CONUS tornadic storms that are of cluster type (Smith et al. 2012). This equation conservatively assumes that the  $POD$  enhancement due to rapid scanning is only effective on cluster storms.

Likewise, for  $FAR$  reduction, a similar logic was applied to arrive at the dashed line shown in Fig. 9. The corresponding equation for 1-min-scan  $FAR$  at  $CHR = 0$  is  $0.33u + a(1 - u)$ , where  $a$  is taken from Table 4. The resulting changes to the curves in Figs. 4 and 9 were applied in computing model results for rapid-scan scenarios.

*f. CONUS grid computation*

We now combine the development presented in the previous sections to produce model estimates of the mean annual casualty cost due to tornadoes over the CONUS. The modeled tornado casualty rate (per year, per grid cell) is given by

$$R_{ijm}^{F,H,R} = \sum_{m=0}^5 [r_{ijm}(1)B_{ijm} + r_{ijm}(0)(1 - B_{ijm})]O_{ijm}Y_{ijm}^{F,H,R}, \quad (5)$$

where  $B$  is the probability of warning per tornado,  $O$  is the tornado occurrence rate,  $i$  and  $j$  are the latitude and longitude grid indices,  $m$  is the EF number, and the superscripts  $F, H,$  and  $R$  denote fatal, injured—hospitalized,

and injured—treated and released, respectively. The casualty type fractions are parsed as

$$Y_{ijm}^F = f_m, \quad (6)$$

$$Y_{ijm}^H = (1 - f_m)h_{ijm}, \quad \text{and} \quad (7)$$

$$Y_{ijm}^R = (1 - f_m)(1 - h_{ijm}), \quad (8)$$

where  $f$  is the fatality fraction given by Table 6 and  $h$  is the fraction of injured that are hospitalized (e.g., Fig. 10). From (2),

$$r_{ijm}(W) = \exp[\alpha \ln(D_{ij}A_{0m}) + \beta \ln S_m + \gamma M_{ij} + \delta F_{ij} + \varepsilon W + k] \quad (9)$$

is the casualty rate per tornado with ( $W = 1$ ) and without ( $W = 0$ ) warning.  $F$  is the gridded  $FAR$  computed from our model via  $CHR$  and the relationship depicted in Fig. 9. The coefficients are given in the upper rows of Table 5;  $D$  is the population density,  $A_0$  is the mean tornado path area, and  $S$  is the mean tornado surface dissipation energy density (Table 6). To include as many years as possible, the tornado occurrence rate maps were generated from the 1950–2016 tornado database downloaded from the NWS SPC’s “SVRGIS” page (<http://www.spc.noaa.gov/gis/svrgis/>). Data from 1950 to 1953 were excluded because of suspected quality issues (Ashley and Strader 2016). Tornadoes were sorted into EF number and  $1^\circ \times 1^\circ$  latitude–longitude bins, and then the annual occurrence rates were bilinearly interpolated to our model grid.

Summing (5) across all grid indices and EF numbers yielded the predicted CONUS tornado casualty rate per year parsed by casualty type. The results were multiplied by the corresponding costs in Table 7 and summed to arrive at the total estimated annual CONUS tornado casualty costs.

*g. False-alarm and sheltering cost reduction*

As demonstrated, tornado warnings save lives. However, they can also exact a cost due to time spent sheltering by people who responded to the warnings. In strict terms, time spent sheltering when a tornado does not hit your building is time wasted. Since very few buildings are actually damaged by tornadoes, that adds up to a lot of lost time.

For a more nuanced take on this issue, we posit that

$$C_S = C_W + C_P, \quad (10)$$

where  $C_S$  is false-alarm sheltering cost,  $C_W$  is cost of lost work time, and  $C_P$  is cost of lost personal time

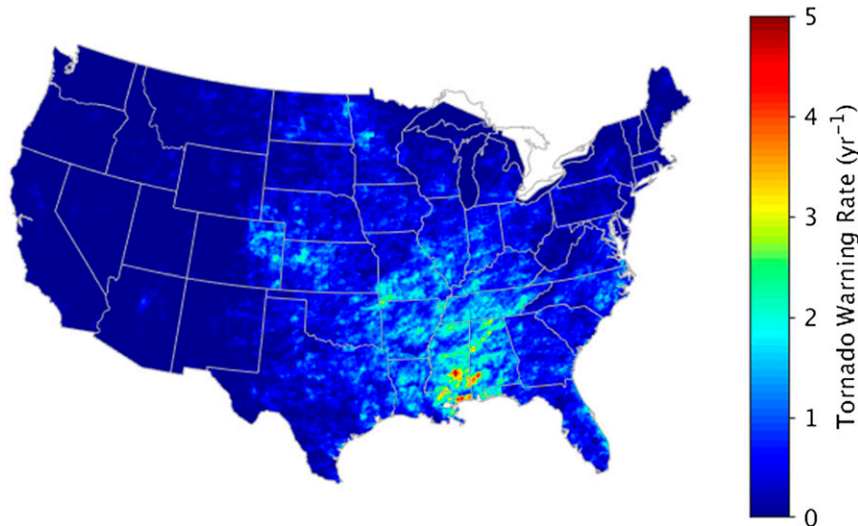


FIG. 11. Mean annual tornado warning issuance rate over the storm-based warning era (October 2007–December 2017).

(all in units of dollars per hour). The  $C_W$  is actually independent of whether a tornado warning is correct or a false alarm—the cost to society from loss of work time does not depend on the outcome of the warning. However, we argue that  $C_P$  becomes zero if the tornado warning was not a false alarm. That is, if one took shelter on a warning and a tornado touched down in the warning area, then one is likely to say that time spent sheltering was worthwhile from a personal perspective. Thus, tornado warning FAR reduction can also generate benefits via decreasing sheltering costs.

The mean per-person cost of work time lost while sheltering can be computed as

$$C_W = F_E F_W V_W, \quad (11)$$

where  $F_E$  is the fraction of the population that is employed,  $F_W$  is fraction of time spent working by those who are employed, and  $V_W$  is the mean wage per hour. The mean per-person cost of personal time lost while sheltering can be calculated as

$$C_P = F_E(1 - F_W)V_P + (1 - F_E)V_P, \quad (12)$$

where  $V_P$  is the value of personal time per unit time. We followed Sutter and Erickson (2010) in valuing personal time as  $1/3$  of the mean wage ( $V_W/3$ ), after Cesario (1976). The latest available (May 2018) total private sector employment numbers were taken from the BLS (<https://www.bls.gov/ces/>) to get  $F_E = 0.627$ ,  $F_W = (34.5 \text{ h week}^{-1}) / (168 \text{ h week}^{-1}) = 0.205$ ,  $V_W = \$26.9 \text{ h}^{-1}$ , and  $V_P = V_W/3 = \$8.97 \text{ h}^{-1}$ . Plugging these values into (10), (11), and (12), we get  $C_S = \$11.28 \text{ h}^{-1}$ .

The total annual added cost of sheltering due to tornado false alarms is given by

$$C_F = HTC_S \sum_{i,j}^{CONUS} I_{ij} P_{ij} F_{ij}, \quad (13)$$

where  $H$  is the shelter response rate,  $T$  is the mean time spent sheltering,  $I$  is the tornado warning issuance rate per year,  $P$  is population, and  $F$  is the modeled false-alarm ratio for tornado warnings. Again, following Sutter and Erickson (2010), we assumed  $H = 0.4$ . We approximated the mean time spent sheltering by the mean tornado warning valid period computed over the storm-based warning era, which yielded  $T = 0.559 \text{ h}$ . The CONUS map of  $I$  for the storm-based warning era is shown in Fig. 11. The CIESIN 2015 and 2020 gridded population data were interpolated to get current (2018) values.

#### 4. Example results

We computed modeled tornado casualty and false-alarm costs for five CONUS radar network configurations: 1) no radar coverage; 2) WSR-88Ds; 3) WSR-88Ds and TDWRs; 4) WSR-88Ds, TDWRs, and a future weather radar at select locations; and 5) perfect radar coverage. Configuration 3 is the current baseline. Configuration 1 allows an estimate of the benefit added by any radars. We computed this case by setting  $FVO = 0$  and  $CHR = \infty$  everywhere. Configuration 2 yields the incremental benefit of TDWRs for tornadoes. Configuration 5 allows an estimate of the remaining benefit

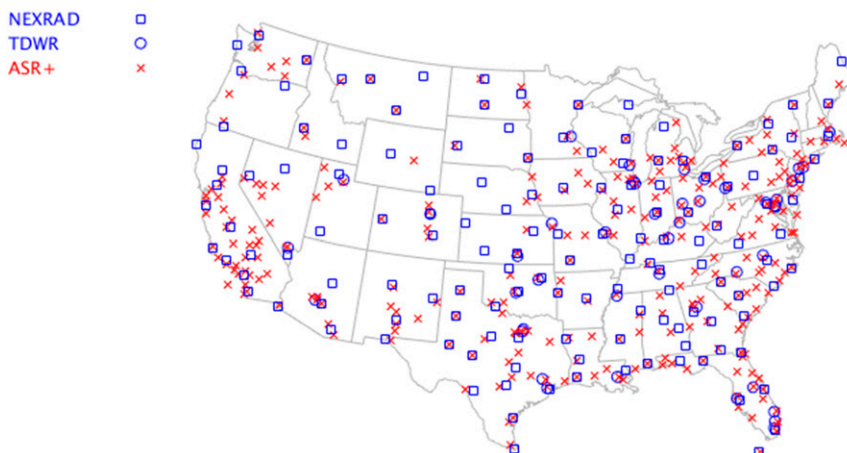


FIG. 12. Locations of radars included in this study.

pool over the current baseline. This case was handled by setting  $FVO = 1$  and  $CHR = 0$  everywhere. Rapid-scanning capability was added to the baseline and perfect coverage configurations for a total of seven cases.

For configuration 4, we tried a scenario in which the current airport surveillance radars (ASRs) are replaced by a multimission radar that we dub ASR+ that is capable of high-quality weather observation. This is one potential future outcome under the ongoing Spectrum Efficient National Surveillance Radar (SENSR) program (FAA 2016). For this radar, we assumed a  $2^\circ$  antenna beamwidth and maximum elevation angle of  $60^\circ$ . Figure 12 shows the locations of all radar types. We also computed costs for all radars upgraded with rapid-scanning (1-min volume update) capability.

Table 9 gives the tornado casualty estimates for all scenarios, as well as the actual average annual casualty rates. (The anomalous April 2011 tornado super outbreak that produced over 3000 casualties skews the means high.) There is excellent agreement between the baseline model results and the actual

casualty rates. Table 10 lists the corresponding tornado casualty costs, and Table 11 adds the estimated costs due to time spent sheltering on false alarms. All costs are in 2018 dollars.

Cost differences from the current baseline (WSR-88D and TDWR) are listed in the “delta baseline” columns of Tables 9–11. Relative to a CONUS without weather radars, the current baseline provides nearly half a billion dollars in tornado benefits annually. The incremental benefit of TDWRs is modest at about  $\$8M\ yr^{-1}$ , which is not surprising since they mostly cover the same areas as the WSR-88Ds. Adding rapid-scanning capability achieves far greater cost reduction than improving radar coverage—just upgrading the existing radars with rapid scanning yields about the same benefit ( $\sim\$100M\ yr^{-1}$ ) as blanketing the CONUS with perfect radar coverage. Most of the rapid-scan benefit derives from tornado warning FAR reduction—this can be seen by comparing the differences between the solid and dashed lines in Figs. 4 and 9. In Fig. 4, the increase in POD due to rapid scanning is very small, and it is only for EF0–1 tornadoes, which generate little casualty cost. In Fig. 9, the

TABLE 9. Annual CONUS tornado casualty estimates. Actual average injured counts are totals and are not broken out by injury type.

Scenario	Fatal	Injured (hospitalized)	Injured (treated and released)	Total	Delta baseline
No radar coverage	81.0	545.3	495.6	1122.0	206.7
WSR-88D	67.4	452.5	398.0	917.8	2.5
WSR-88D and TDWR	67.2	451.3	396.8	915.3	—
WSR-88D, TDWR, and rapid scan	64.6	434.3	381.5	880.4	−34.9
WSR-88D, TDWR, and ASR+	66.8	448.4	393.9	909.0	−6.3
WSR-88D, TDWR, ASR+, and rapid scan	64.1	430.6	377.9	872.6	−42.7
Perfect coverage	64.5	432.9	375.9	873.3	−42.0
Perfect coverage and rapid scan	60.9	408.9	358.4	828.2	−87.1
Actual mean (1998–2017)	$82 \pm 26$		$1105 \pm 257$	$1187 \pm 283$	—
Actual median (1998–2017)	$50 \pm 11$		$788 \pm 126$	$850 \pm 135$	—

TABLE 10. Annual CONUS tornado casualty cost estimates.

Scenario	Fatal (\$M)	Injured (hospitalized) (\$M)	Injured (treated and released) (\$M)	Total (\$M)	Delta baseline (\$M)
No radar coverage	872.1	1560.7	250.7	2683.4	468.2
WSR-88D	724.7	1295.0	201.3	2221.0	5.8
WSR-88D and TDWR	722.9	1291.7	200.7	2215.2	—
WSR-88D, TDWR, and rapid scan	695.4	1243.0	192.9	2131.3	−83.9
WSR-88D, TDWR, and ASR+	718.3	1283.3	199.2	2200.7	−14.5
WSR-88D, TDWR, ASR+, and rapid scan	689.6	1232.5	191.1	2113.2	−102.0
Perfect coverage	693.8	1239.0	190.1	2122.9	−92.3
Perfect coverage and rapid scan	655.4	1170.3	181.2	2006.9	−208.3

reduction in FAR due to rapid scanning is much more significant. Tornado warning FAR is high ( $\sim 0.72$ ) relative to other severe weather warnings. For example, in the mid-2000s, NWS warning FARs were 0.46 for flash floods, 0.31 for winter storms, 0.31 for high winds, and 0.48 for severe thunderstorms (Barnes et al. 2007). There has been a slow decrease in FAR in recent years as a result of an apparent increased focus on this issue (Brooks and Correia 2018), but there is still room for improvement (although POD should not be sacrificed for this purpose). Also, if the connection between casualty reduction and longer lead times can be established, then the benefit estimates for rapid scanning will rise even more.

There is a caveat with the rapid-scanning results. Since there are no operational weather radars conducting volume scans at a rate of one per minute, our rapid-scan FAR reduction model was necessarily based on a limited number of experiments carried out with the NWRT phased array radar. Other parts of our cost model were based on large numbers of tornadoes and warnings (Tables 1 and 3), inspiring a much higher degree of confidence. Since the overall results indicated high benefit leverage through rapid scanning, it would be prudent to gather more statistics on the effects of faster volume scans on tornado warning performance by utilizing existing and new radars capable of fine temporal resolution observations (e.g., Kurdzo et al. 2017; Stailey and Hondl 2016).

Maps of cost density could also be used to analyze optimal locations for new gap-filling radars (e.g., Kurdzo and Palmer 2012). Figure 13 shows the cost density difference between the current baseline and perfect coverage (without rapid scanning), which shows the areas with the largest remaining benefit pools. Although the small-scale details are dominated by the high dynamic range of the population density, and much of the larger-scale modulation is due to tornado occurrence rate, the radar coverage deficiencies are also visible, for example, the honeycomb-like pattern in the Midwest. Of course, this is only for tornadoes, so similar maps should be generated for other key cost generators such as flash floods.

Figure 13 seems to indicate that virtually all of the CONUS tornado benefit pool exists east of the Rocky Mountains. To show this explicitly, we computed the annual tornado casualty and false-alarm cost estimates for the CONUS east of 106°W longitude (Table 12). The “delta baseline” column is almost identical to the one in Table 11.

## 5. Summary discussion

In this study, we developed a geospatial model for calculating weather radar benefits for tornadoes. We showed that certain radar performance and coverage metrics impacted tornado warning statistics (detection

TABLE 11. Annual CONUS tornado casualty and false-alarm cost estimates.

Scenario	Casualty (\$M)	False-alarm sheltering (\$M)	Total (\$M)	Delta baseline (\$M)
No radar coverage	2683	288	2971	492
WSR-88D	2221	266	2487	8
WSR-88D and TDWR	2215	264	2479	—
WSR-88D, TDWR, and rapid scan	2131	234	2365	−114
WSR-88D, TDWR, and ASR+	2201	262	2463	−16
WSR-88D, TDWR, ASR+, and rapid scan	2113	230	2343	−136
Perfect coverage	2123	255	2378	−101
Perfect coverage and rapid scan	2007	214	2221	−258

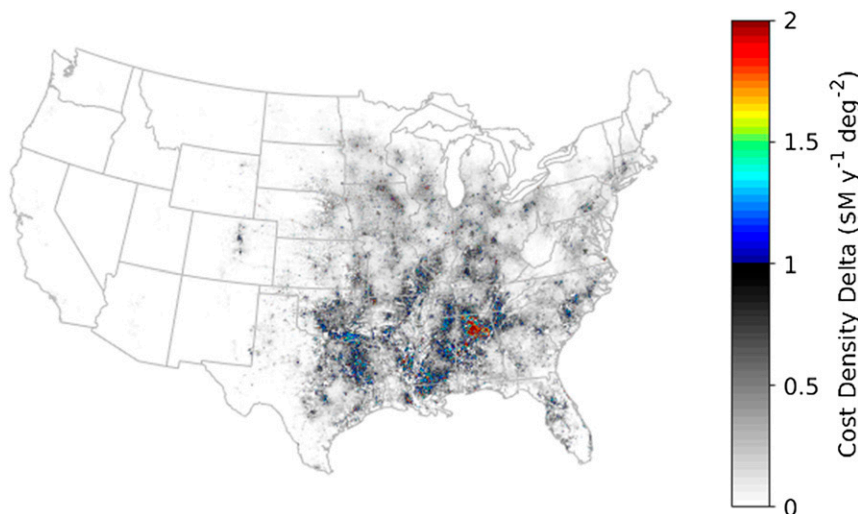


FIG. 13. Modeled annual tornado cost density (casualty plus warning false-alarm costs) difference between the current weather radar network configuration and perfect radar coverage (no rapid scanning).

probability and false-alarm ratio), which, in turn, affected casualty rate and loss of work and personal time in sheltering (Fig. 14). The model operates on a high-resolution spatial grid over the CONUS capable of revealing regional variances. It can take as input any hypothetical radar network configuration.

The “fraction of vertical volume observed” measure of radar network coverage is new to tornado warning performance analysis. It takes into account the near-range cone of silence, the far-range loss of low-level coverage due to Earth’s curvature, as well as terrain blockage and ground height variability. It was instrumental in establishing an unambiguously positive correlation between radar coverage and tornado warning performance.

Our model showed that the current weather radar network provides a benefit of nearly 0.5 billion dollars per year with respect to tornadoes. There is a remaining benefit pool of over \$250Myr<sup>-1</sup>. This pool is divided almost equally between improved coverage and faster scanning. Since perfect coverage (or anything close to it)

would be extremely expensive, upgrading existing sites with faster-scanning radars may be a more cost-effective way to harvest more of those benefits (for tornadoes). However, we must note that the quantification of rapid-scan effects was based on a small number of experiments and is less robust than the other parts of our benefit model.

Tornado warning FAR is positively correlated with casualty rate and incurs added cost because of work and personal time lost during sheltering. Reducing the current FAR of 0.72 is a worthy goal that taps into this benefit. However, making progress in this direction is complicated and involves much more than improving weather radar data.

As discussed earlier, tornadoes are just one type of hazardous weather to consider when planning a weather radar network and executing a business case analysis for it. We are currently conducting a study that is similar to this one but for quantitative precipitation estimation performance, and we will be developing a benefit model for flash floods.

TABLE 12. Annual tornado casualty and false-alarm cost estimates east of the Rockies.

Scenario	Casualty (\$M)	False-alarm sheltering (\$M)	Total (\$M)	Delta baseline (\$M)
No radar coverage	2678	283	2961	490
WSR-88D	2217	262	2479	8
WSR-88D and TDWR	2211	260	2471	—
WSR-88D, TDWR, and rapid scan	2127	230	2357	-114
WSR-88D, TDWR, and ASR+	2197	258	2455	-16
WSR-88D, TDWR, ASR+, and rapid scan	2109	227	2336	-135
Perfect coverage	2119	251	2370	-101
Perfect coverage and rapid scan	2003	210	2213	-258

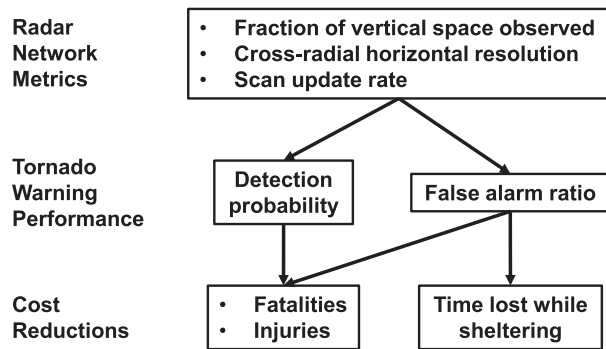


FIG. 14. Simplified diagram of the weather radar tornado benefits model.

**Acknowledgments.** We sincerely thank the following people: Chris Miller for acquiring and processing the housing-type data; Don Burgess, Pam Heinselman, Harold Brooks, and Walker Ashley for providing valuable technical guidance; Jud Stailey for help in forming the initial outline of this study; the NWS forecasters who responded to our survey regarding TDWR usage; Jerry Brotzge and two anonymous referees for discerning critiques of the initial typescript; and Kurt Hondl and Mark Weber for supporting this project. This paper has been approved for public release: distribution is unlimited. This material is based upon work supported by the National Oceanic and Atmospheric Administration under Air Force Contract FA8702-15-D-0001. Any opinions, findings, conclusions, or recommendations expressed in this material are those of the authors and do not necessarily reflect the views of the National Oceanic and Atmospheric Administration.

## REFERENCES

- Ashley, W. S., and S. M. Strader, 2016: Recipe for disaster: How the dynamic ingredients of risk and exposure are changing the tornado disaster landscape. *Bull. Amer. Meteor. Soc.*, **97**, 767–786, <https://doi.org/10.1175/BAMS-D-15-00150.1>.
- Barnes, L. R., E. C. Gruntfest, M. H. Hayden, D. M. Schultz, and C. Benight, 2007: False alarms and close calls: A conceptual model of warning accuracy. *Wea. Forecasting*, **22**, 1140–1147, <https://doi.org/10.1175/WAF1031.1>.
- Bieringer, P., and P. S. Ray, 1996: A comparison of tornado warning lead times with and without NEXRAD Doppler radar. *Wea. Forecasting*, **11**, 47–52, [https://doi.org/10.1175/1520-0434\(1996\)011<0047:ACOTWL>2.0.CO;2](https://doi.org/10.1175/1520-0434(1996)011<0047:ACOTWL>2.0.CO;2).
- Brooks, H. E., and J. Correia Jr., 2018: Long-term performance metrics for National Weather Service tornado warnings. *Wea. Forecasting*, **33**, 1501–1511, <https://doi.org/10.1175/WAF-D-18-0120.1>.
- Brotzge, J., and S. Erickson, 2009: NWS tornado warnings with zero or negative lead times. *Wea. Forecasting*, **24**, 140–154, <https://doi.org/10.1175/2008WAF2007076.1>.
- , and —, 2010: Tornadoes without NWS warning. *Wea. Forecasting*, **25**, 159–172, <https://doi.org/10.1175/2009WAF2222270.1>.
- , and W. Donner, 2013: The tornado warning process: A review of current research, challenges, and opportunities. *Bull. Amer. Meteor. Soc.*, **94**, 1715–1733, <https://doi.org/10.1175/BAMS-D-12-00147.1>.
- , K. Hondl, B. Philips, L. Lemon, E. J. Bass, D. Rude, and D. L. Andra, 2010: Evaluation of distributed collaborative adaptive sensing for detection of low-level circulations and implications for severe weather warning operations. *Wea. Forecasting*, **25**, 173–189, <https://doi.org/10.1175/2009WAF2222233.1>.
- , S. Erickson, and H. Brooks, 2011: A 5-yr climatology of tornado false alarms. *Wea. Forecasting*, **26**, 534–544, <https://doi.org/10.1175/WAF-D-10-05004.1>.
- , S. E. Nelson, R. L. Thompson, and B. T. Smith, 2013: Tornado probability of detection and lead time as a function of convective mode and environmental parameters. *Wea. Forecasting*, **28**, 1261–1276, <https://doi.org/10.1175/WAF-D-12-00119.1>.
- Brown, R. A., and V. T. Wood, 2012a: Simulated vortex detection using a four-face phased-array Doppler radar. *Wea. Forecasting*, **27**, 1598–1603, <https://doi.org/10.1175/WAF-D-12-00059.1>.
- , and —, 2012b: The tornadic signature: An update. *Wea. Forecasting*, **27**, 525–530, <https://doi.org/10.1175/WAF-D-11-00111.1>.
- , —, and D. Sirmans, 2002: Improved tornado detection using simulated and actual WSR-88D data with enhanced resolution. *J. Atmos. Oceanic Technol.*, **19**, 1759–1771, [https://doi.org/10.1175/1520-0426\(2002\)019<1759:ITDUSA>2.0.CO;2](https://doi.org/10.1175/1520-0426(2002)019<1759:ITDUSA>2.0.CO;2).
- Burgess, D. W., and L. R. Lemon, 1990: Severe thunderstorm detection by radar. *Radar in Meteorology*, D. Atlas, Ed., Amer. Meteor. Soc., 619–647.
- Cesario, F. J., 1976: Value of time in recreation benefit studies. *Land Econ.*, **52**, 32–41, <https://doi.org/10.2307/3144984>.
- Cho, J. Y. N., 2015: Revised Multifunction Phased Array Radar (MPAR) network siting analysis. MIT Lincoln Laboratory Project Rep. ATC-425, 84 pp., [https://www.ll.mit.edu/sites/default/files/publication/doc/2018-05/Cho\\_2015\\_ATC-425.pdf](https://www.ll.mit.edu/sites/default/files/publication/doc/2018-05/Cho_2015_ATC-425.pdf).
- , and M. E. Weber, 2010: Terminal Doppler weather radar enhancements. *Proc. 2010 IEEE Radar Conf.*, Washington, DC, Institute of Electrical and Electronics Engineers, <https://doi.org/10.1109/RADAR.2010.5494427>.
- Chrisman, J. N., 2013: Dynamic scanning. *NEXRAD Now*, No. 22, NOAA/NWS/Radar Operations Center, Norman, OK, 1–3, <https://www.roc.noaa.gov/WSR88D/PublicDocs/NNOW/NNOW22c.pdf>.
- , 2014: The continuing evolution of dynamic scanning. *NEXRAD Now*, No. 23, NOAA/NWS/Radar Operations Center, Norman, OK, 8–13, <http://www.roc.noaa.gov/WSR88D/PublicDocs/NNOW/NNOW23a.pdf>.
- CIESIN, 2017: Population density, v4.10 (2000, 2005, 2010, 2015, 2020). Gridded Population of the World (GPW), v4, NASA Socioeconomic Data and Applications Center, Center for International Earth Science Information Network, Columbia University, Palisades, NY, <https://doi.org/10.7927/H4DZ068D>.
- Edwards, R., and H. E. Brooks, 2010: Possible impacts of the enhanced Fujita scale on United States tornado data. *25th Conf. on Severe Local Storms*, Denver, CO, Amer. Meteor. Soc., P8.28, <http://ams.confex.com/ams/pdfpapers/175398.pdf>.
- FAA, 2016: Spectrum Efficient National Surveillance Radar (SENSR) program announcement. Federal Aviation Administration Solicitation 25214, AAQ-300, <https://faaco.faa.gov/index.cfm/announcement/view/25214>.
- Fabry, F., 2015: *Radar Meteorology: Principles and Practice*. Cambridge University Press, 256 pp.



- Falk, K. W., 1997: Techniques for issuing severe thunderstorm and tornado warnings with the WSR-88D Doppler radar. NOAA Tech. Memo. NWS SR-185, 38 pp., <https://repository.library.noaa.gov/view/noaa/6360>.
- FEMA, 2009: FEMA benefit–cost analysis reengineering (BCAR): Tornado safe room module methodology report, version 4.5. Federal Emergency Management Administration Rep., 75 pp., <https://www.fema.gov/media-library-data/20130726-1738-25045-0690/tornadomethodology.pdf>.
- Fricker, T., J. B. Elsner, and T. H. Jagger, 2017: Population and energy elasticity of tornado casualties. *Geophys. Res. Lett.*, **44**, 3941–3949, <https://doi.org/10.1002/2017GL073093>.
- Gibbs, J. G., 2016: A skill assessment of techniques for real-time diagnosis and short-term prediction of tornado intensity using the WSR-88D. *J. Oper. Meteor.*, **4**, 170–181, <https://doi.org/10.15191/nwajom.2016.0413>.
- Heinselman, P. L., and S. M. Torres, 2011: High-temporal-resolution capabilities of the National Weather Radar Testbed Phased-Array Radar. *J. Appl. Meteor. Climatol.*, **50**, 579–593, <https://doi.org/10.1175/2010JAMC2588.1>.
- , D. L. Priegnitz, K. L. Manross, T. M. Smith, and R. W. Adams, 2008: Rapid sampling of severe storms by the National Weather Radar Testbed Phased Array Radar. *Wea. Forecasting*, **23**, 808–824, <https://doi.org/10.1175/2008WAF2007071.1>.
- , D. S. LaDue, D. M. Kingfield, and R. Hoffman, 2015: Tornado warning decisions using phased-array radar data. *Wea. Forecasting*, **30**, 57–78, <https://doi.org/10.1175/WAF-D-14-00042.1>.
- Istok, M. J., A. Cheek, A. D. Stern, R. E. Saffle, B. R. Klein, N. Shen, and W. M. Blanchard, 2009: Leveraging multiple FAA radars for NWS operations. *25th Int. Conf. on Interactive Information and Processing Systems for Meteorology, Oceanography, and Hydrology*, Phoenix, AZ, Amer. Meteor. Soc., 10B.2, <https://ams.confex.com/ams/pdfpapers/145466.pdf>.
- Kurdzo, J. M., and R. D. Palmer, 2012: Objective optimization of weather radar networks for low-level coverage using a genetic algorithm. *J. Atmos. Oceanic Technol.*, **29**, 807–821, <https://doi.org/10.1175/JTECH-D-11-00076.1>.
- , and Coauthors, 2017: Observations of severe local storms and tornadoes with the atmospheric imaging radar. *Bull. Amer. Meteor. Soc.*, **98**, 915–935, <https://doi.org/10.1175/BAMS-D-15-00266.1>.
- Lemon, L. R., and C. A. Doswell III, 1979: Severe thunderstorm evolution and mesocyclone structure as related to tornado-genesis. *Mon. Wea. Rev.*, **107**, 1184–1197, [https://doi.org/10.1175/1520-0493\(1979\)107<1184:STEAMS>2.0.CO;2](https://doi.org/10.1175/1520-0493(1979)107<1184:STEAMS>2.0.CO;2).
- Manson, S., J. Schroeder, D. Van Riper, and S. Ruggles, 2018: IPUMS National Historical Geographic Information System, version 13.0. University of Minnesota, accessed 11 June 2018, <http://doi.org/10.18128/D050.V13.0>.
- McLaughlin, D., and Coauthors, 2009: Short-wavelength technology and the potential for distributed networks of small radar systems. *Bull. Amer. Meteor. Soc.*, **90**, 1797–1818, <https://doi.org/10.1175/2009BAMS2507.1>.
- Michelson, M., W. W. Shrader, and J. G. Wieler, 1990: Terminal Doppler Weather Radar. *Microwave J.*, **33**, 139–148.
- Moran, M. J., and C. Monje, 2016: Guidance on treatment of the economic value of a statistical life (VSL) in U.S. Department of Transportation Analyses—2016 adjustment. Department of Transportation Memo., 13 pp., <https://cms.dot.gov/sites/dot.gov/files/docs/2016%20Revised%20Value%20of%20a%20Statistical%20Life%20Guidance.pdf>.
- NOAA, 2018: Natural hazard statistics. NWS Office of Climate, Water, and Weather Services, <http://www.nws.noaa.gov/om/hazstats.shtml>.
- NRC, 2002: *Weather Radar Technology beyond NEXRAD*. National Research Council, National Academy Press, 81 pp., <https://doi.org/10.17226/10394>.
- Press, W. H., S. A. Teukolsky, W. T. Vetterling, and B. P. Flannery, 1992: *Numerical Recipes in C: The Art of Scientific Computing*. 2nd Ed. Cambridge University Press, 994 pp.
- Ramsdell, J. V., Jr., and J. P. Rishel, 2007: Tornado climatology of the contiguous United States. U.S. Nuclear Regulatory Commission Office of Nuclear Regulatory Research Tech. Rep. NUREG/CR-4461, Rev. 2, 257 pp., <https://www.nrc.gov/docs/ML0708/ML070810400.pdf>.
- Schultz, C. J., and Coauthors, 2012: Dual-polarization tornadic debris signatures, Part I: Examples and utility in an operational setting. *Electron. J. Oper. Meteor.*, **13** (9), 120–137, <http://nwafiles.nwas.org/ej/pdf/2012-EJ9.pdf>.
- Simmons, K. M., and D. Sutter, 2005: WSR-88D radar, tornado warnings, and tornado casualties. *Wea. Forecasting*, **20**, 301–310, <https://doi.org/10.1175/WAF857.1>.
- , and —, 2008: Tornado warnings, lead times, and tornado casualties: An empirical investigation. *Wea. Forecasting*, **23**, 246–258, <https://doi.org/10.1175/2007WAF2006027.1>.
- , and —, 2009: False alarms, tornado warnings, and tornado casualties. *Wea. Climate Soc.*, **1**, 38–53, <https://doi.org/10.1175/2009WCAS1005.1>.
- , and —, 2011: *Economic and Societal Impact of Tornadoes*. Amer. Meteor. Soc., 282 pp.
- Smith, B. T., R. L. Thompson, J. S. Grams, C. Broyles, and H. E. Brooks, 2012: Convective modes for significant severe thunderstorms in the contiguous United States. Part I: Storm classification and climatology. *Wea. Forecasting*, **27**, 1114–1135, <https://doi.org/10.1175/WAF-D-11-00115.1>.
- Staley, J. E., and K. D. Hondl, 2016: Multifunction Phased Array Radar for aircraft and weather surveillance. *Proc. IEEE*, **104**, 649–659, <https://doi.org/10.1109/JPROC.2015.2491179>.
- Sutter, D., and S. Erickson, 2010: The time cost of tornado warnings and the savings with storm-based warnings. *Wea. Climate Soc.*, **2**, 103–112, <https://doi.org/10.1175/2009WCAS1011.1>.
- Torres, S., and C. Curtis, 2006: Design considerations for improved tornado detection using superresolution data on the NEXRAD network. Preprints, *Third European Conf. on Radar Meteorology and Hydrology (ERAD)*, Barcelona, Spain, Amer. Meteor. Soc., 5B.10, <https://ams.confex.com/ams/pdfpapers/116240.pdf>.
- USCB, 2016: B25033: Total population in occupied housing units by tenure by units in structure. 2011–2015 American Community Survey 5-Year Estimates, U. S. Census Bureau, accessed 11 June 2018, <http://factfinder2.census.gov>.
- Weber, M. E., J. Y. N. Cho, J. S. Herd, J. M. Flavin, W. E. Benner, and G. S. Torok, 2007: The next-generation multimission U.S. surveillance radar network. *Bull. Amer. Meteor. Soc.*, **88**, 1739–1751, <https://doi.org/10.1175/BAMS-88-11-1739>.
- Wilson, K. A., P. L. Heinselman, C. M. Custer, D. M. Kingfield, and Z. Kang, 2017: Forecaster performance and workload: Does radar update time matter? *Wea. Forecasting*, **32**, 253–274, <https://doi.org/10.1175/WAF-D-16-0157.1>.
- Wood, V. T., and R. A. Brown, 1997: Effects of radar sampling on single-Doppler velocity signatures of mesocyclones and tornadoes. *Wea. Forecasting*, **12**, 928–938, [https://doi.org/10.1175/1520-0434\(1997\)012<0928:EORSOS>2.0.CO;2](https://doi.org/10.1175/1520-0434(1997)012<0928:EORSOS>2.0.CO;2).
- Zrnich, D. S., and R. J. Doviak, 1976: Effective antenna pattern of scanning radars. *IEEE Trans. Aerosp. Electron. Syst.*, **AES-12**, 551–555, <https://doi.org/10.1109/TAES.1976.308254>.